Egyptian Journal of Chemistry

http://ejchem.journals.ekb.eg/

Optimization and Performance Analysis of Dye-Sensitized Solar Cells Using SCAPS-1D: Comparative Study of Layer and Blend Configurations with Enhanced Efficiency through SnO2 Integration

M. A. Abd El Ghany*[1], M. D. Asham[1], W. Abdelaziz[2], Walid Soliman[1], and Tarek M. Abdolkader[1]
[1]Department of Basic Engineering Sciences, Benha Faculty of Engineering, Benha University, Benha, Egypt
[2] Department of Electrical and Electronic Engineering, Faculty of Engineering, May University in Cairo (MUC), Egypt

---

Abstract

For their low cost and environmental friendliness, dye sensitized solar cells (DSSC) are becoming more widely used as a yet strongly evolving strain of solar cells. In this paper development of a simulation based on two different models (layer and blend configurations) is made using SCAPS-1D. The two structures of DSSC employed in this work are composed of (1) (the fluorine tin oxide) FTO/(titanium dioxide) TiO_2/ (the metal-free organic dye) MK_2 dye/(polymer gel electrolyte) PGE/(platinum) pt and (2) FTO/TiO_2 & MK_2 dye/PGE/pt respectively. The effect of ETL (electron transport layer) and HTL (hole transport layer) thicknesses, working temperature, doping in ETL, electron mobility, and defect density at interface between active layer and HTM on different parameters of the DSSC are studied. In each case open circuit voltage (V_{oc}), short circuit current density (J_{sc}), fill factor (FF), and power conversion efficiency (PCE) parameters are analyzed. The obtained results are contrasted with those of experiments indicating that using blend configuration yields a better concurring behavior compared to the layer configuration. Optimization process has been done on the blend structure increasing the efficiency from 5.5109 % up to 16.2702 %. A novel dye sensitized solar cell structure is reported in this paper replacing titanium dioxide (TiO_2) with stannic oxide (SnO_2) commended by its characteristic superiority raising the cell efficiency to 19.77 %. The outcomes demonstrate that this innovative DSSC structure has promising commercialization potential.

Keywords: Dye sensitized solar cells; polymer gel electrolyte (PGE); Electron transport layer (ETL); J–V characteristics; SCAPS-1D

---

1. Introduction

Nowadays, researchers are drawn to OSCs (organic solar cells) because of their affordability, rapid improvement of low-temperature manufacturing methods and power conversion efficiency (PCE) [1]. Among different OSC generations, dye-sensitized solar cells' is the most widely used architecture for its potentially low-cost alternativeness to that of silicon. This is ascribed to its ease of fabrication and higher efficiency suitability for commercial applications [2, 3]. A sensitizing dye is used in a simple manufacturing technique to capture light and produce electrons in DSSCs (dye sensitized solar cells). One of the advantages of these cells is the ability to harvest light effectively even at comparatively low temperatures [4, 5]. Additionally, by substituting solid polymer electrolytes for liquid electrolytes, the major problems of employing liquid electrolytes are now eliminated by creating quasi-solid dye-sensitized solar cells. The fact that DSSCs can be utilized indoors and even at night is one of their benefits. The intriguing surface characteristics and chemical stability of TiO_2 nanostructures, including nanospheres, nanorods, and nanotubes, make them effective photoanode materials for DSSC. Gratzel and O'Regan characterized the first DSSC [2], and by resolving an electron transport diffusion equation, the J–V (current density-voltage) properties were ascertained. Numerous researchers have built and examined a number of models based on this. Ferber created [2] an electrical model that combines interfacial chemical interactions with the physical charge transport process. In order to study the DSSC I–V characteristics under inhomogeneous excitation of TiO_2, Muto and Suzuki created a straightforward model [2]. There are several works of literature exist on DSSC modelling and experimental validation. In order to understand the photo-electrical features of DSSC, Ahalya Gunasekaran et al. [6] provided an experimental study that we have simulated and calibrated in this paper. In this work, the physical arrangement has been modelled through two different methodologies: the layer and the blend methodologies. Both have been investigated via studying the effect of ETL and HTL thicknesses, defect density at interface layers, doping concentration and electron mobility of ETL and working temperature on the cell performance. In this work, efficiency, fill factor, short circuit current, and open circuit voltage have been assessed. The theoretical simulation's output is verified by comparing

---

*Corresponding author e-mail: menallah.abdelghani@bhit.bu.edu.eg.; (Menallah Samy Mohamed Abd Elghany).
Receive Date: 14 January 2025, Revise Date: 27 February 2025, Accept Date: 04 March 2025
DOI: 10.21608/ejchem.2025.352944.11165

it with published experimental data. The theoretical values for calibration show close agreement with the experimental ones. It is found that the blend structure is more accurate and adherent faithful to the original construction than that of layer structure throughout the process of parameters tuning. In this work, the blend methodology has been optimized. A novel structure has been developed by replacing TiO_2 with SnO_2 as the ETL layer.

2. Methodology

Any software that can numerically solve the fundamental semiconductor equations can simulate solar cell devices. A number of simulation tools, including AFORS-HET, SILVACO ATLAS, GPVDM, and wxAMPS, have been used to assess PSC performance [2, 7]. SCAPS version 3.3.07 has been used in this work. It is a one-dimensional solar cells capacitance simulator [1, 6]. It has the capability of analysing hetero- and multi-junction photovoltaic devices with acceptable results that highly agree with physical cell behaviour [7]. In the bulk of a semiconductor layer, three recombination mechanisms [6] may be identified with SCAPS: Auger, band-to-band (direct), and SRH with defect levels being specified at the interface or across the body of the material.

Common measurements like current-voltage and quantum efficiency (QE) are evaluated by solving the two primary equations, Poisson's (1) and continuity equations for electrons and holes (2&3) [5, 7]. All simulations in this work are performed in the AM 1.5 spectrum with global illumination and an incident power density of 85 mW/cm^2.

$$\frac{d}{dx}\left(\varepsilon(x)\frac{d\Psi}{dx}\right) = q\,[\,p\,(x) - n\,(x) + ND^{+}(x) - NA^{-}(x) + pt\,(x) - nt\,(x)] \qquad (1)$$

$$\frac{\partial p}{\partial t} = -\frac{1}{q}\frac{\partial Jp}{dx} - Rp\,(x) + G\,(x) \qquad (2)$$

$$\frac{\partial n}{\partial t} = \frac{1}{q}\frac{dJn}{dx} - Rn\,(x) + G\,(x) \qquad (3)$$

Where: ε is the dielectric permittivity, q is the charge of electron, Ψ is the electrostatic potential, p is the free holes, n is the free electrons, p_t and n_t are the trapped holes and electrons, N_A^- and N_D^+ are the ionized acceptor and donor as doping concentrations, R_p and R_n are the hole and electron recombination rates, G is the generation rate, and J_p and J_n are the hole and electron current densities.

3. Simulation Framework

The calibrated cell's configuration, shown in Fig. 1 (a) Layer structure configuration: consists of five typical layers: (FTO), ETL (TiO_2), (MK_2 dye) active layer, HTL (PGE), and the back contact (pt). (b) Blend structure configuration: consists of four layers: the fluorine tin oxide (FTO), the blend layer (TiO_2 & MK_2 dye), HTL (PGE), and the back contact (pt). (c) HOMO (higher order molecular orbital)–LUMO (lower order molecular orbital) band diagram of the two different methodologies

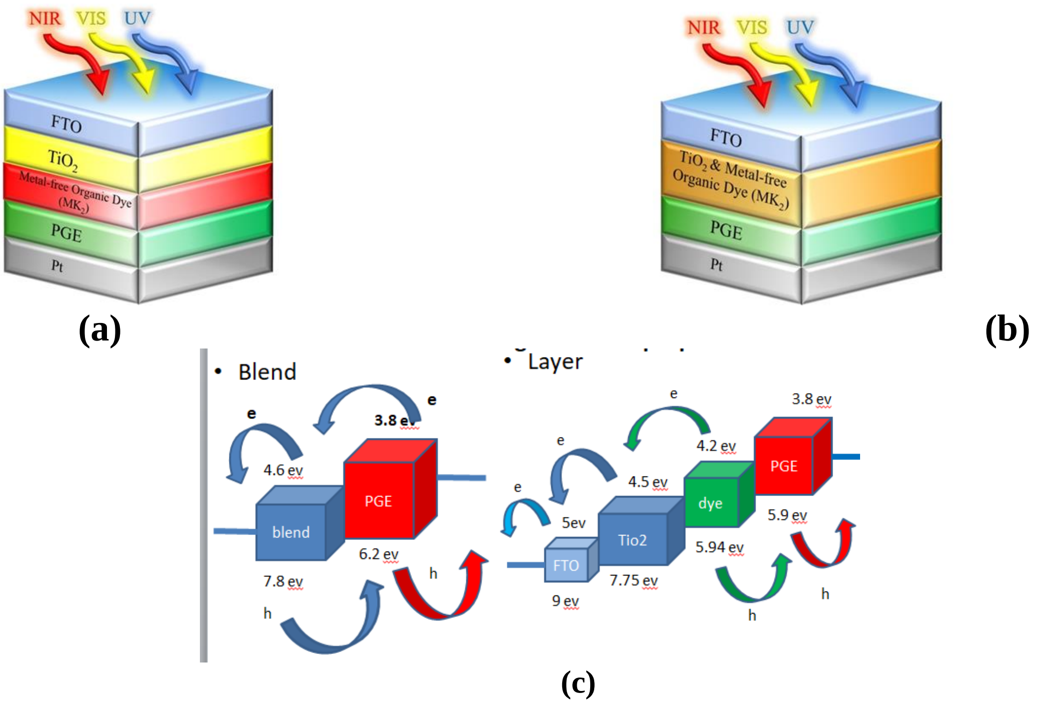

Fig. 1. The main structures of the simulated cells exhibiting (a) layer structure, (b) blend structure, and (c) HOMO–LUMO band diagram.

The primary physical parameters of the layers of the two configurations defined in the simulation are shown in **Table. 1**.

Table. 1 List of Parameters used in simulation [4 - 8]

	Parameters for Layer configuration			
Parameters	FTO	TiO$_2$	MK$_2$ Dye	PGE
Thickness W (μm)	0.1	55	8	55
Bandgap E_g (eV)	4	3.2	1.74	2.4
Electron affinity χ (eV)	5	4.5	4.2	3.8
Dielectric permittivity ε_r	9	10	30	55
Effective density of states for CB N_c (cm^{-3})	$2.2X10^{18}$	$1x10^{19}$	$1x10^{20}$	$1x10^{19}$
Effective density of states for VB N_v (cm^{-3})	$1.8X10^{19}$	$1x10^{19}$	$1x10^{20}$	$1x10^{19}$
Electron mobility μ_n (cm^2/Vs)	$2X10^{1}$	$2.5x10^{5}$	$5x10^{1}$	$5x10^{1}$
Hole mobility μ_p (cm^2/Vs)	$1X10^{1}$	$5x10^{2}$	$5x10^{1}$	$1x10^{5}$
Shallow uniform donor density N_D (cm^{-3})	10^{19}	$1x10^{10}$	10^{15}	0
Shallow uniform acceptor density N_A (cm^{-3})	$1X10^{1}$	0	10^{15}	$1x10^{18}$
Defect type	Neutral	Neutral	Neutral	Neutral
Defect density N_t (cm^{-3})	$1x10^{14}$	$2x10^{13}$	$1x10^{13}$	$1x10^{13}$

	Parameters for blend configuration		
Parameters	FTO	TiO$_2$&dye (blend)	PGE
Thickness W (μm)	0.1	55	55
Bandgap E_g (eV)	4	3.2	2.4
Electron affinity χ (eV)	5	4.6	3.8
Dielectric permittivity ε_r	9	10	55
Effective density of states for CB N_c (cm^{-3})	$2.2X10^{18}$	$1x10^{19}$	$1x10^{17}$
Effective density of states for VB N_v (cm^{-3})	$1.8X10^{19}$	$1x10^{16}$	$1x10^{20}$
Electron mobility μ_n (cm^2/Vs)	$2X10^{1}$	$1x10^{3}$	$1x10^{2}$
Hole mobility μ_p (cm^2/Vs)	$1X10^{1}$	$3x10^{1}$	$5x10^{1}$
Shallow uniform donor density N_D (cm^{-3})	10^{19}	$2x10^{18}$	0
Shallow uniform acceptor density N_A (cm^{-3})	$1X10^{1}$	$1x10^{1}$	$1x10^{18}$
Defect type	Neutral	Neutral	Neutral
Defect density N_t (cm^{-3})	$1x10^{14}$	$1x10^{15}$	$1x10^{13}$

4. Results and Discussion

The experimental data (PGE J10) published by Ahalya Gunasekaran et al. [6] is used to validate the theoretical simulation's results. These results logically concur with the experimentally current-voltage characteristics, as seen in **Fig. 2**

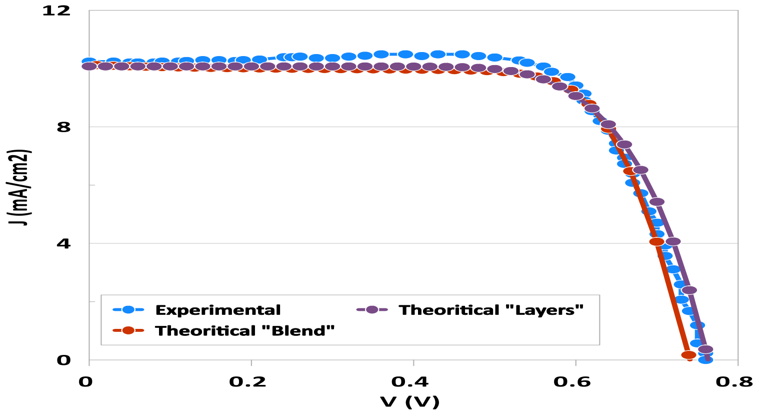

Fig. 2. Calibration of dye sensitized solar cell Illuminated I-V curve by two different configurations

Following the cell calibration, an investigation is conducted into how technological parameters affect the cell's output in order to maximize its efficiency and determine how much more efficiency may be improved. The parameters that were examined are the blend thickness, the doping density of blend layer, the HTL thickness, the operating temperature, electron mobility in blend layer, and trap density in the blend/PGE interface.

4.1 The effect of the ETL thickness

When it comes to dye-sensitized solar cells' stability, efficiency, and other PV metrics, the thickness of the ETL layer is vital. Few studies have examined how variations in ETL thickness affect cell performance [2, 9]. In the blend structure, as thickness increases, J_{SC}, V_{oc}, and efficiency “η” increase as shown in **Fig. 3 (a, c, g).** This is due to higher surface area being available for dye adsorption [12] thus resulting in the increased electron-hole pair generation in the absorber layer (dye molecules) [11, 12]. The highest rate of photon absorption by the dye and the maximum rate of electron injection from the excited dye to the TiO_2 conduction band are clearly correlated with the parameters peaks being at an optimal thickness [15] near which maximum output power is achieved [12]. Beyond the optimum thickness (75 µm), values of these parameters decline as injected electrons become lost to more traps since transport distance is longer. For simulated DSSC, as thickness increases, the photo-anode's ability to absorb more photons results in a rise in photocurrent density. As electron recombination rate increases with thickness above the optimum value, photocurrent density decreases [10, 11]. Additionally, as charge transfer resistance rises, more injected electrons are lost due to recombination and diffusion length constraint [2].

While in case of the layer structure, it is noticed that Jsc, Voc, and η keep on decreasing as the thickness of Tio_2 increases. The reason for their is the formation of larger pinholes and uneven surface [13], as shown clearly in **Fig. 3 (b, d, h).** Here we make a comparison between layer and blend structure. All the results we obtained are correct, but the layer results do not agree with the practical work of the dye cell. The layer results agree with the results of other cells, for example, perovskite solar cells. Therefore, we explain that simulating Dye cells is preferable using a blend structure method, as its results are consistent with the results of practical research on Dye.

Furthermore, electron back transfer to the electrolyte contributes to lowering V_{oc} with greater thicknesses [12]. In order to balance the diffusion and absorption lengths, the ideal thickness is thus selected [1]. V_{oc} can be defined from **Eqn. (4)** [2] and is dependent on the ratio of the dark generation and dark saturation currents.

$$V_{oc} = \frac{nkT}{q} \ln\left(\frac{Il}{Io} + 1\right) \qquad (4)$$

The dark saturation current falls with increasing thickness. However, in contrast to lower ETL thickness levels, the pace of this decline reduces at larger thickness values. Therefore, it can be concluded that the primary cause of the change in V_{oc} is its reliance on the dark saturation current [2].

The effect of ETL layer thickness on the fill factor is irregular in the investigated domain. The FF decreases as the thickness increases because the series resistance rises with thickness [2]. According to **Eqn. 5**, we can understand how the FF changes with variations of V_{OC}, J_{SC}, maximum current (I_m) and maximum voltage (V_m) and illustrate the relation of FF with the thickness of the ETL layers in both models in **Fig. 3 (e, f)** [16].

$$FF = \frac{Vm * Im}{Voc * Isc} \qquad (5)$$

4.2 The effect of Working Temperature

The influence of the operating temperature on the photovoltaic parameters of the DSSC was measured in the range of 295 to 360 K. The J_{sc} increases with increasing temperature, as shown in **Fig. 4 (a, b)**, mainly due to the increase in conductivity of the electrolyte “HTL” [17] and the decrease of the energy gap of the material [18]. Besides, an increase in temperature also reduces the viscosity of the electrolyte diminishing the diffusion resistance, which is proportional to the viscosity. A small decrease in the open circuit voltage is observed with increasing temperature as shown in **Fig. 4 (c, d)**. Previously, other research groups -based DSSCs, a linear decrease in V_{OC} with temperature was observed [17]. The TiO_2 electrode's band gap narrows with increasing temperature, which results in a smaller difference between the TiO_2 Fermi level and the redox potential of the redox electrolyte, hence a reduced V_{OC}. The device's V_{OC} falls as the temperature rises because it raises the recombination current or dark current [17]. The rate of increasing of J_{SC} caused by thermal generation of carriers [2] is very small compared to the decreasing rate of V_{OC}, thus the efficiency and fill factor of the cell decrease with increasing the cell’s temperature as shown in **Fig. 4 (e, f, g, h)**,

In the end, we note that temperature has the same effect on the behavior of both the blend and layer configurations. We observe that the PCE values are (5.64%, 5.56%) for the blend and layer respectively at temperature (295 K). Therefore, the effect of the working temperature on the blend structure is more efficient than layer structure.

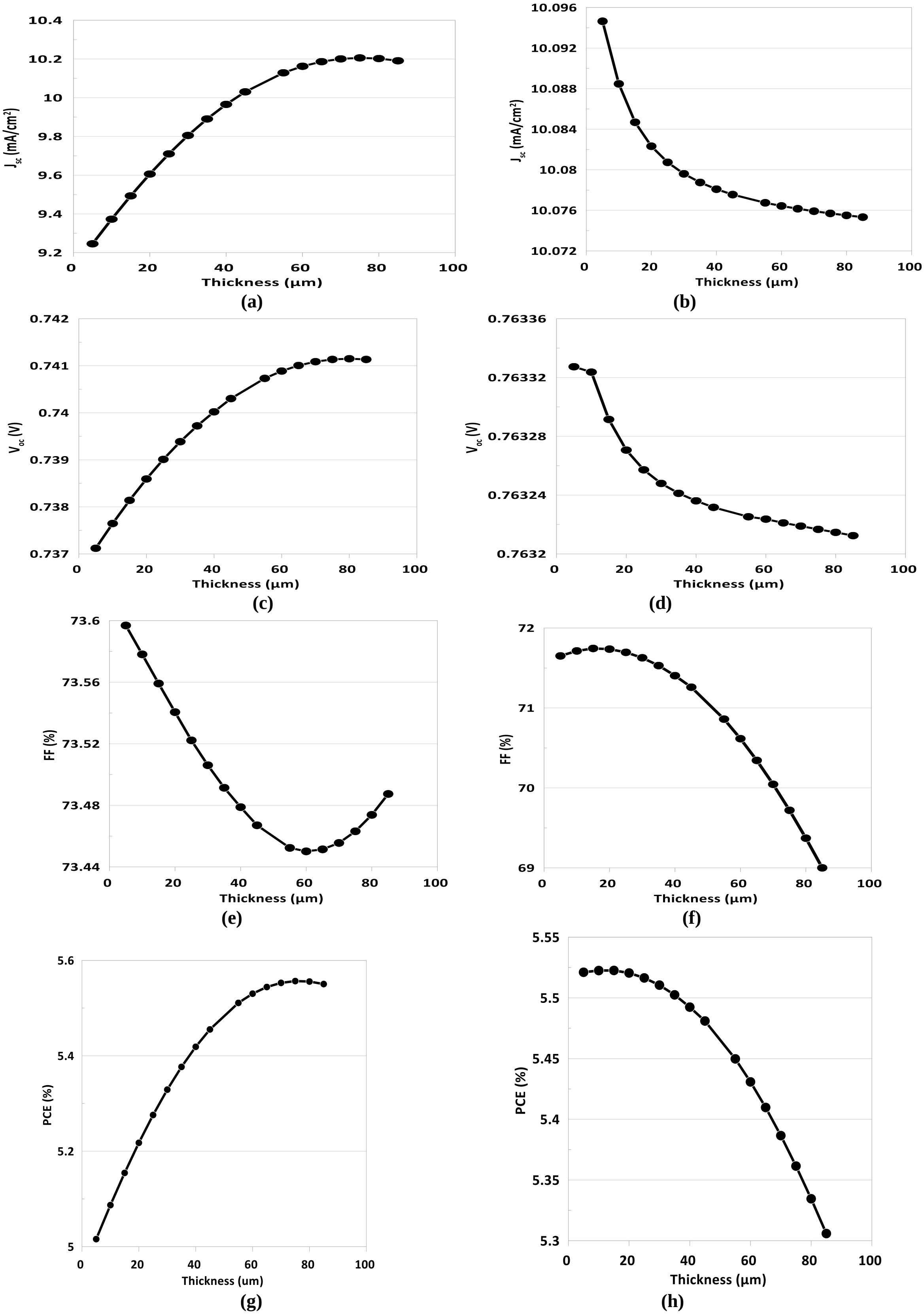

(a) (b)

(c) (d)

(e) (f)

(g) (h)

Blend **Layer**

Fig. 3. Effect of ETL layer thickness variation on (a, b) Jsc, (c, d) Voc, (e, f) FF, and (g, h) PCE for blend and layer structure respectively.

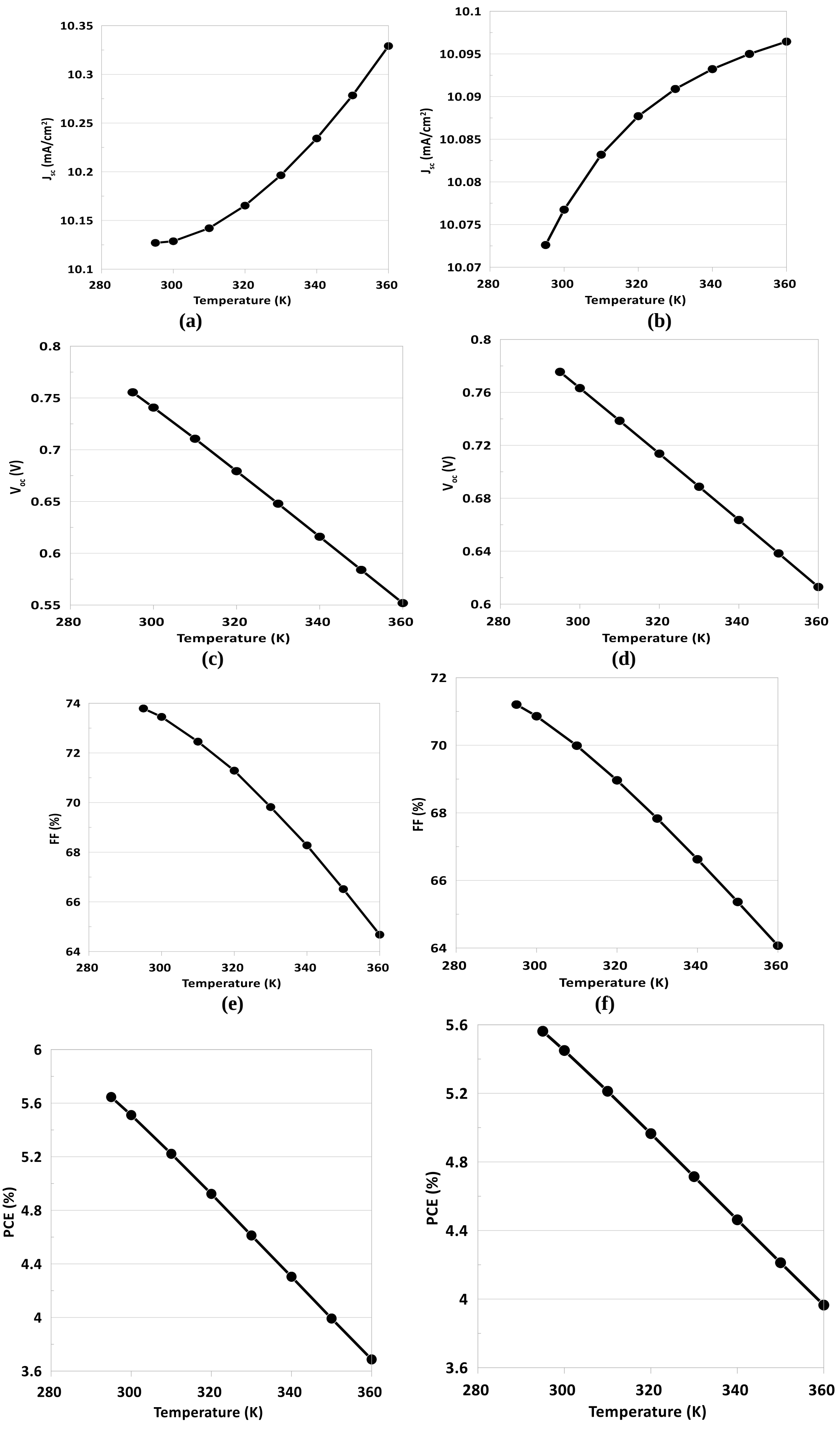
10.35
10.3
10.25
10.2
10.15
10.1
J_{sc} (mA/cm^2)
280
300
320
340
360
Temperature (K)
10.1
10.095
10.09
10.085
10.08
10.075
10.07
J_{sc} (mA/cm^2)
Temperature (K)
0.8
0.75
0.7
0.65
0.6
0.55
V_{oc} (V)
Temperature (K)
0.8
0.76
0.72
0.68
0.64
0.6
V_{oc} (V)
Temperature (K)
74
72
70
68
66
64
FF (%)
Temperature (K)
72
70
68
66
64
FF (%)
Temperature (K)
6
5.6
5.2
4.8
4.4
4
3.6
PCE (%)
Temperature (K)
5.6
5.2
4.8
4.4
4
3.6
PCE (%)
Temperature (K)

(a) **(b)**

(c) **(d)**

(e) **(f)**

(g) **(h)**

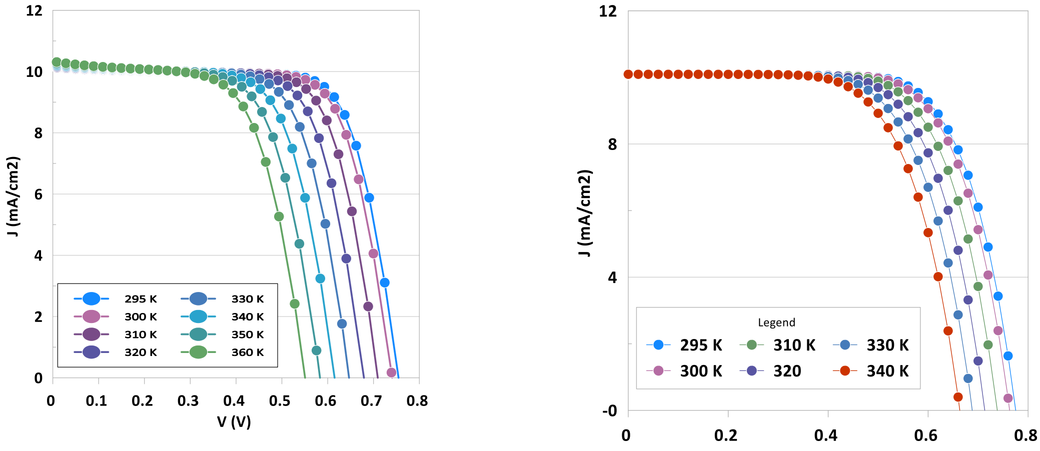

(I) (j)

Blend **Layer**

Fig. 4. Effect of working temperature variation on (a, b) Jsc, (c, d) Voc, (e, f) FF, and (g, h) PCE for blend and layer structure (I, j) J–V curves of simulated cells with varying temperature.

4.3 The effect of the doping density of ETL

Doping density (N_D) of the blend layer in a solar cell can have a major impact on its functionality. The doping concentration of was varied from 1× 10^{12} to 1× 10^{20} cm^{-3} and its effect on the device's performance was observed, as shown in **Fig. 5**. The ETL can be made more conductive by doping it [2]. The series resistance decreases as conductivity increases. Consequently, this lowers carrier recombination losses and improves the DSSC's total current collection performance and efficiency [4]. We choose the doping density range of 10^{12} to 10^{20} cm-3 based on previously published results [17] because the greater dopant concentration may result in the formation of traps, which act as electron–hole recombination centers for TiO_2. It can be seen that the PCE values are (12.005%, 6.97%) for the blend and layer models respectively at doping density 10^{20} cm^{-3}. Therefore, the effect of the doping density on the blend structure is more beneficial than the layer structure.

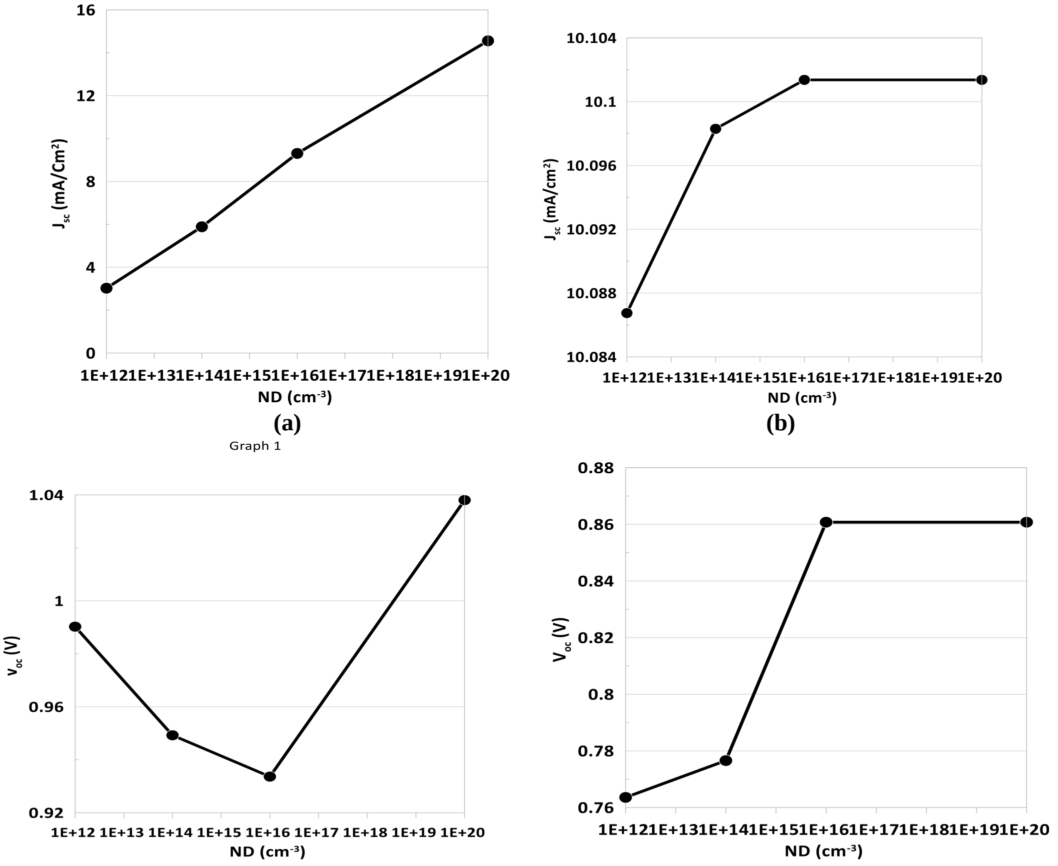

(a) (b)

(c) (d)

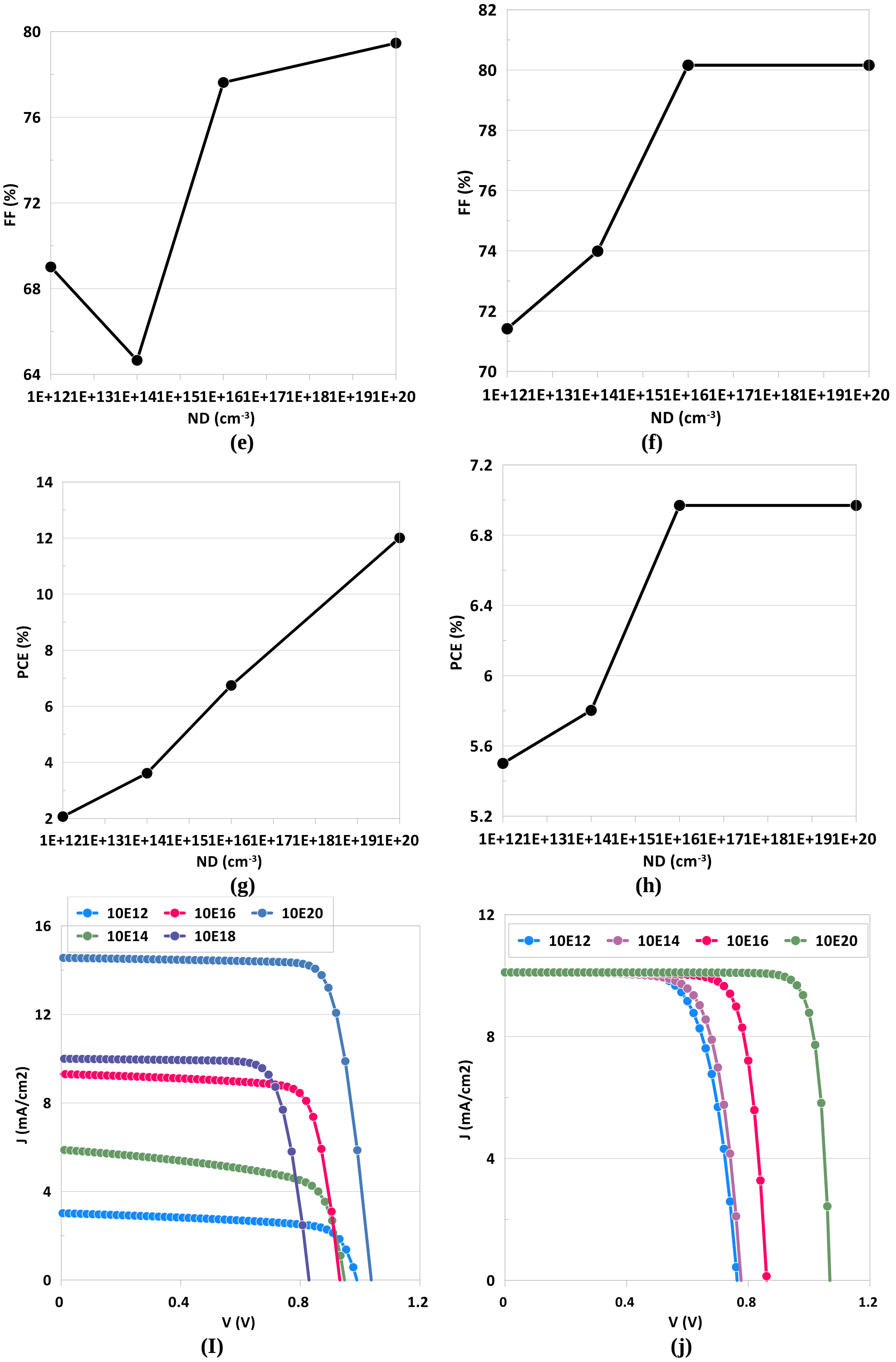

(e)

(f)

(g)

(h)

(I)
Blend

(j)
layer

Fig. 5. Variation of ND of ETL layer with (a, b) J_{sc} (c, d) V_{oc} (e, f) FF (g, h) PCE and (I, j) J–V curves of simulated cells with varying ND

4.4 The effect of the PGE thickness

The effect of PGE thickness on the different parameters of DSSC is demonstrated. The thickness has been changed throughout the range of 40–90 µm and its effect on the V_{OC}, J_{SC}, FF, and η of the DSSC has been observed as shown in **Fig. 6**. V_{OC}, J_{SC}, and PCE increase with the increase of HTM thickness as shown in **Fig. 6 (a, c, g)**. This enhancement is attributable to the exceptional charge transport properties demonstrated by the PGE, this makes charge transfer more effective [3]. Moreover, the enhanced thickness enhances the performance of the DSSCs by improving the interaction between the blend layer and the HTL. The fill factor (FF) declines as the thickness of the PGE layer increases as shown in **Fig. 6 (e)**. This result implies that although the charge transport capabilities are enhanced, the FF may decrease due to an increase in the charge recombination rate or lateral resistance in the device's junction [3, 11].

It is found that the effect of PGE thickness on the short circuit current same for both layer and blend structures, while the other parameters (voc, FF, ɳ) we find that the effect of PGE thickness is incompatible with practical results for layer structure. Therefore, studying the effect of PGE thickness on the blend structure was clearer, more consistent with practical results, and similar to previous research

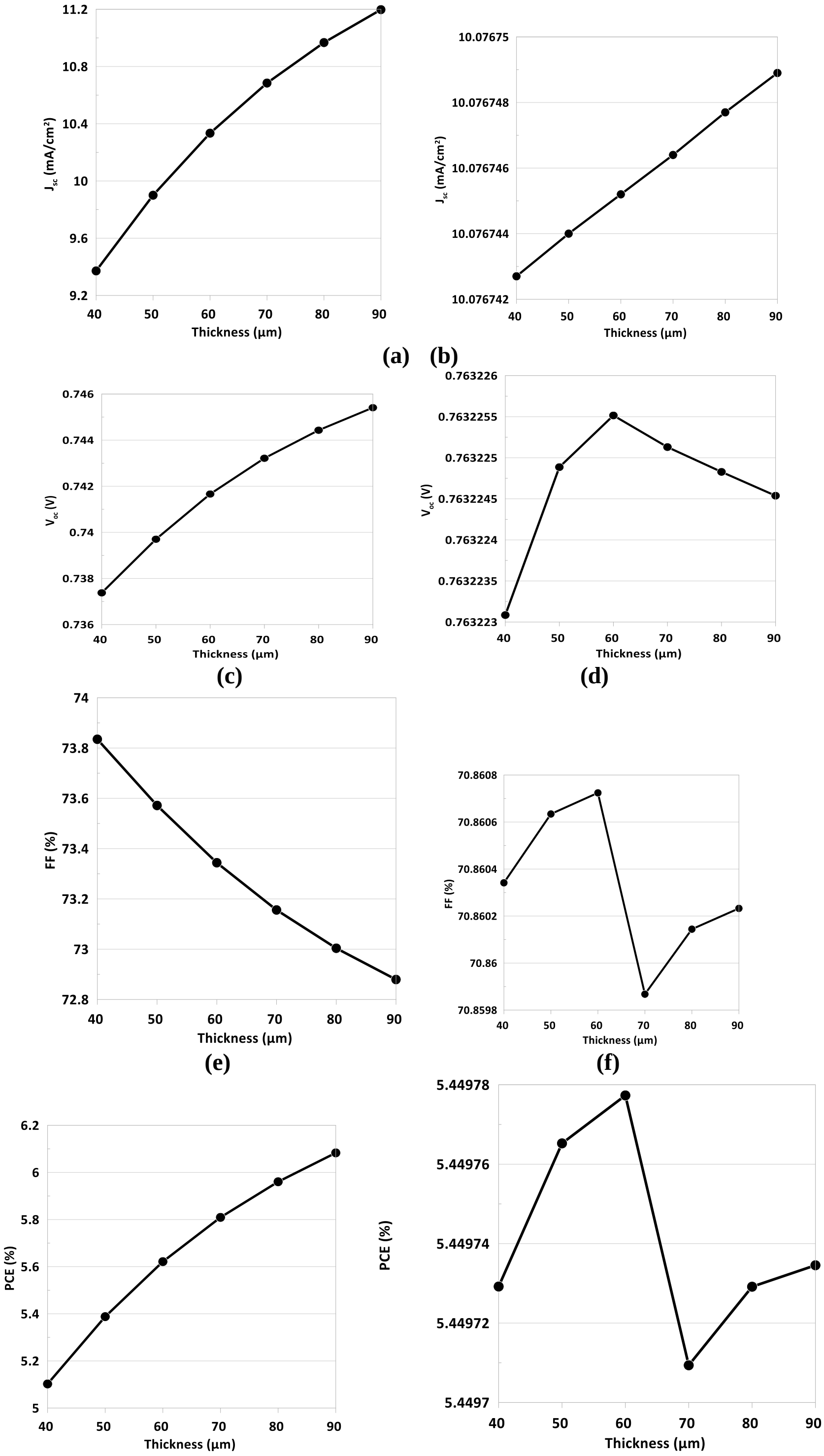

(a) (b)

(c) **(d)**

(e) **(f)**

(g) **(h)**

Blend **layer**

Fig. 6. Effect of HTL layer thickness variation on (a, b) Jsc, (c, d) Voc, (e, f) FF, and (g, h) PCE for blend and layer structure

4.5 The effect of the electron mobility of ETL layer

One of the ruling factors in enhancing the output and results of DSSCs is the charge carrier mobility (μ_e). In this article, charge carrier mobility is altered from 1x 10^1 to 1 x 10^5 cm^2 /Vs to investigate the impact on device performance as shown in **Fig. 7**. The short-circuit current density increases with carrier mobility owing to reduction in dissociation probability, thus, increasing efficiency and FF as shown in **Fig. 7 (a, e, g)** [3]. V_{OC} is approximately at 0.748 V when the mobility is 10 cm^2/Vs and falls to 0.741 V as the mobility is 10^5 cm^2/Vs.

The effect of the electron mobility of ETL layer is almost the same on the behavior of both the blend and the layer configurations. PCE values are 5.56%, 5.33% for the blend and the layer models respectively at electron mobility of 10^5 cm^2/Vs showing that the effect of the electron mobility of the ETL layer on the blend structure is more effectively beneficial than on the layer structure.

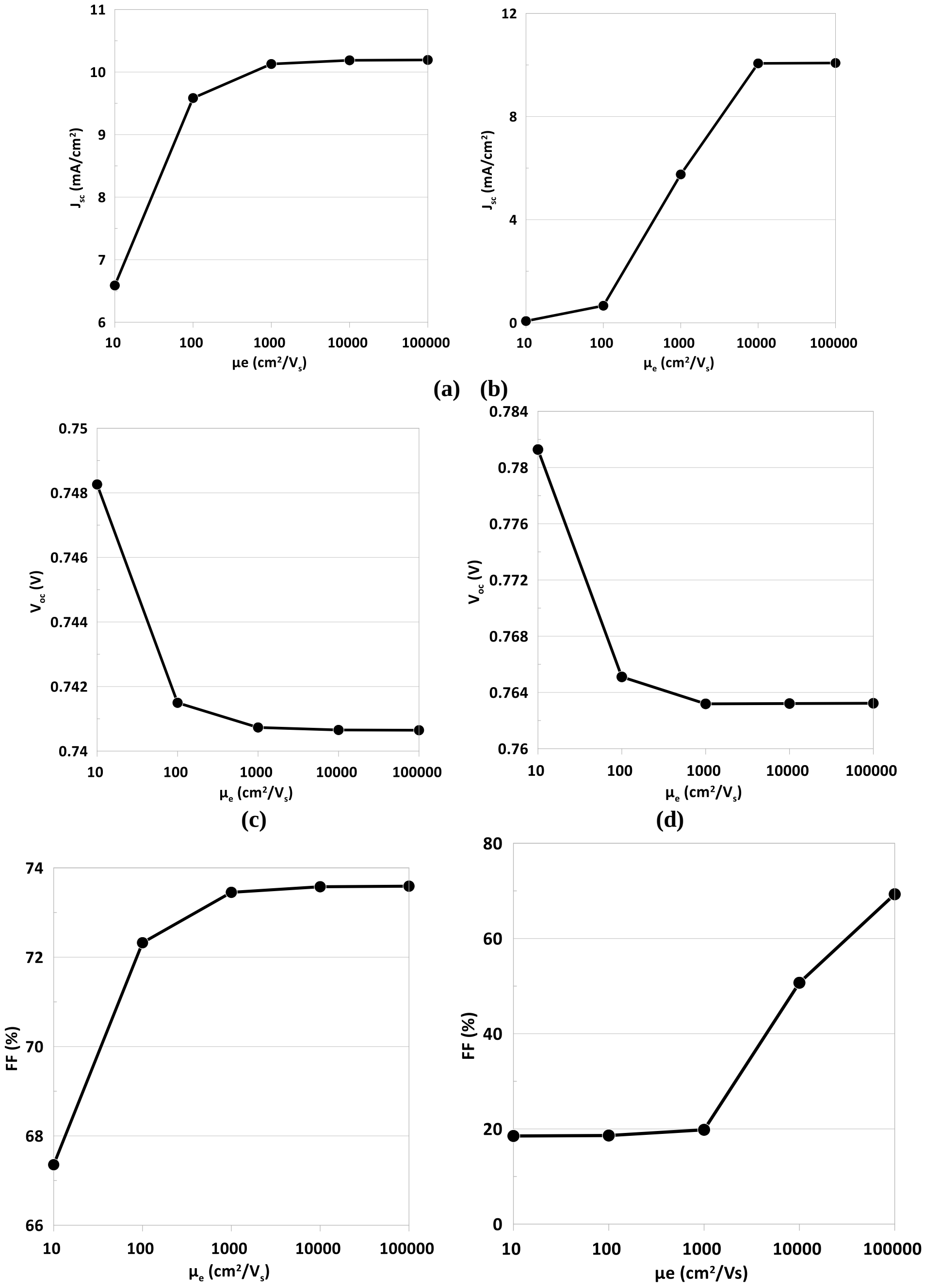

(a) (b)

(c) (d)

(e) (f)

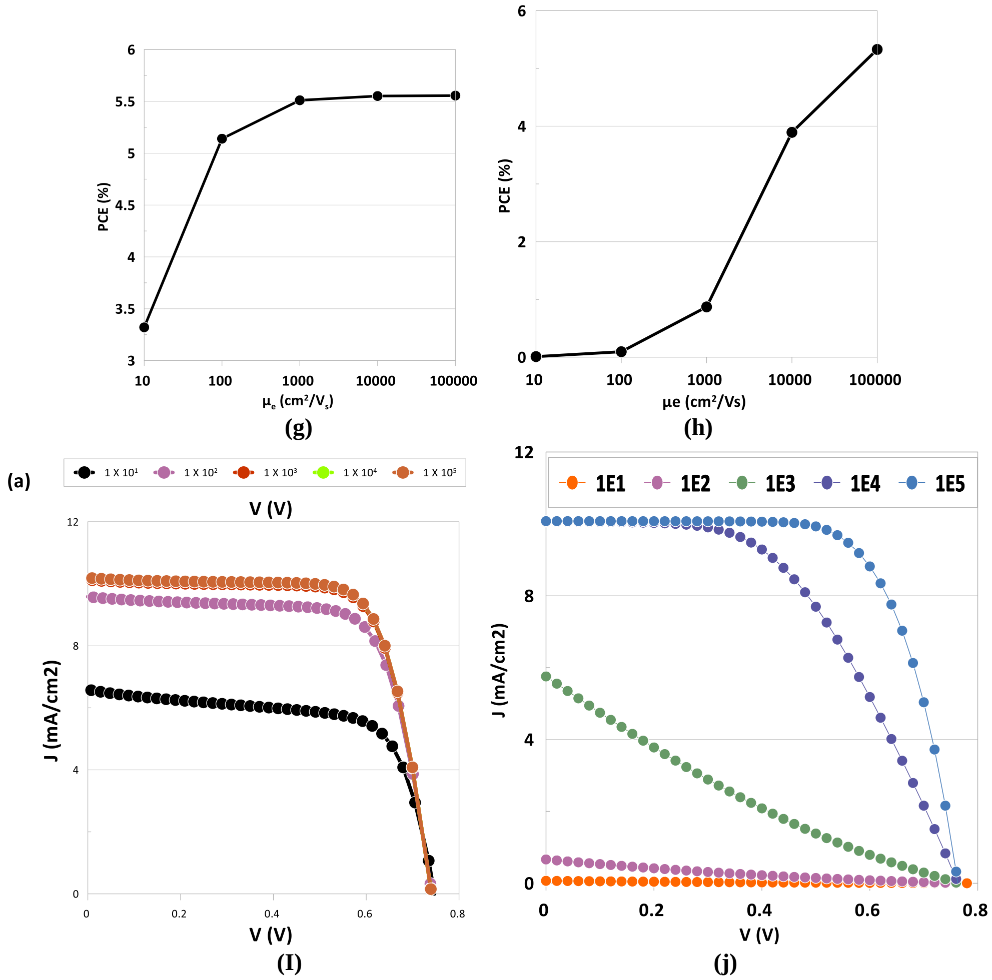

(g) (h)

(I) (j)

Blend layer

Fig. 7. Variation of electron mobility with (a, b) J$_{sc}$ (c, d) V$_{oc}$ (e, f) FF (g, h) PCE and (I, j) J–V curves of simulated cells with varying μ$_{e}$

4.6 The impact of interface layer defect density

The impact of recombination caused by the blend/PGE and MK2 dye/PGE interfaces defects for blend and layer structures respectively is also investigated as shown in **Fig. 8**. In simulation setup, the defect density is varied from 7×10^{16} cm^{-2} to 7×10^{20} cm^{-2}. **Fig. 8** demonstrates the properties of the simulated cell with various interface defect concentrations. Interface flaws significantly affect cell performance, as **Fig. 8** makes abundantly clear. Cell performance deteriorates as a result of the increased defect densities, which provide additional recombination centers and traps. Electrons or holes may become imprisoned in trap states, which are localized energy levels within the active layer material's bandgap. An electron or hole that becomes stuck in a trap state is unable to produce electricity. This lowers the carrier lifetime and, as a result, increases recombination, which lowers the efficiency of both solar cell architectures. Obviously, improved device performance can be introduced by lowering defect densities to 7×10^{16} cm^{-2} at which the PCE for the blend and the layer structures are 10.83%, 5.44% respectively [2].

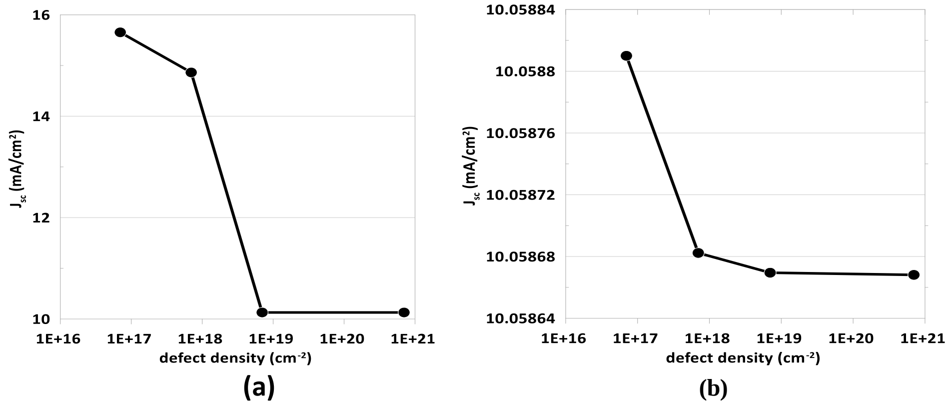

(a) (b)

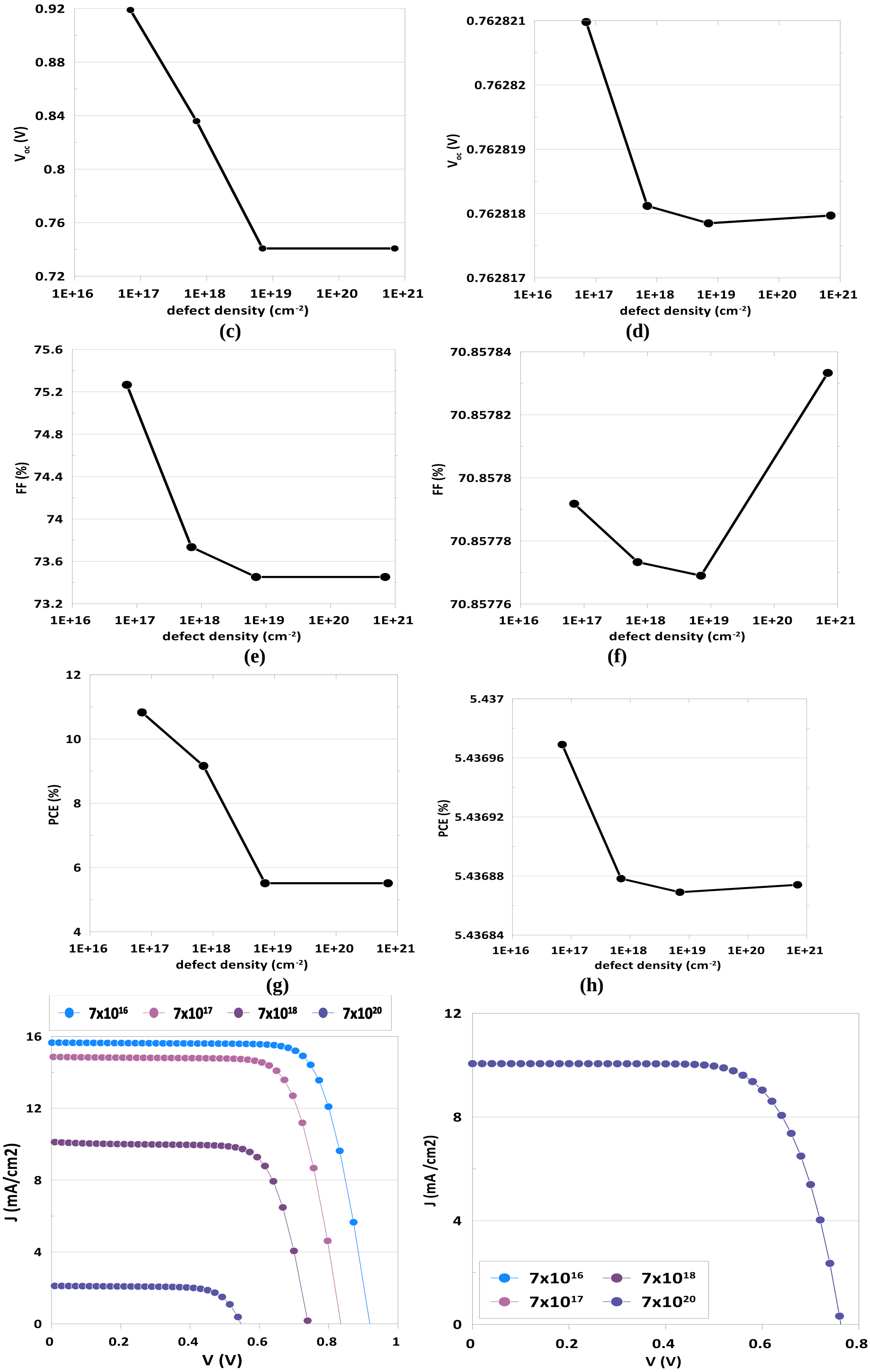

(c) (d)

(e) (f)

(g) (h)

(I) Blend

(j) layer

Fig. 8 Variation of defect density at interface layer with (a, b) J_{sc} (c, d) V_{oc} (e, f) FF (g, h) PCE and (I, j) J–V curves of simulated cells with varying N_t

5. Optimization of the Blend Structure

In the above sub-sections, the thicknesses of ETL and HTL are varied to perform the study that showcases their influence on the PV parameters of the solar cell. Doping density of the ETL layer, defect density at the interfaces, electron mobility at the ETL layer and working temperature are also inspected showing their effects on the performance of the device. Following a thorough examination of all the impacts, the blend device is chosen and optimized for the best-obtained values to produce the finest possible output [19]. The optimized J-V curve for the blend device along with all the PV parameters are shown in **Fig. 9**. **Table 2** for the exact reported PV parameter outcomes is also presented.

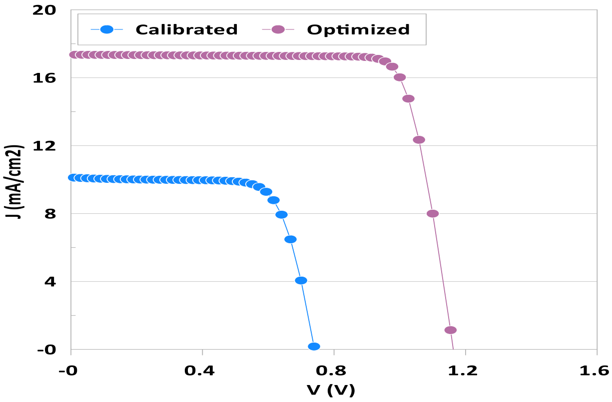

Fig. 9 J-V characteristic curves of the calibrated and optimized blend structure solar cell

Table. 2 the performance experimental, calibrated, and optimized parameters of the device.

	Jsc (mA/cm^2)	Voc (V)	FF (%)	PCE (%)
Experimental	10.2	0.758	73	5.64
Calibrated	10.12869	0.7407	73.4523	5.5109
Optimized	17.3542	1.16289	80.6211	16.2702

6. Improvement of the Dye Sensitized Solar Cell

A novel structure is proposed to improve PCE of dye sensitized solar cell (DSSCs). The composition of the photoanode substrate and the shape of the TiO_2 or SnO_2 films are important determinants of the efficiency and short circuit current. In comparison to conventional semi-conductors, TiO_2 and SnO_2 oxides have a high band gap (3–4 eV), good acid resistance, low cost, easy production, availability, strong thermal stability, and great optical quality [20]. These properties make them appealing materials for several applications such as solar cells [21]. SnO_2 has been thoroughly studied in many successful PSC states because of its advantageous characteristics, which include high mobility and a wide bandgap. Several studies show that the performances of the solar cell with SnO_2 are higher than that with TiO_2. Sno_2 showed UV-resistance properties, excellent chemical stability, and less photocatalytic activity in comparison with TiO_2 or other ETLs, This is beneficial for device stability.

In the current proposal, TiO_2 is replaced with SnO_2 for the new dye sensitized solar cell structure. **Fig. 10** shows current – voltage curve for the blend configuration using TiO_2 and SnO_2 as the ETL layers for DSSCs. Parameters of the new structure are demonstrated in **Table 3**. Results show that this structure may be viable for commercialization in the near future.

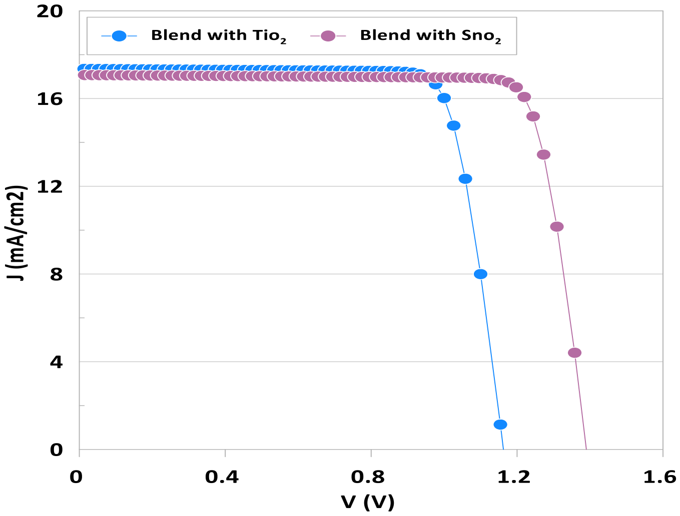

Fig. 10 J-V curve of the novel dye sensitized solar cell by replacing TiO_2 with SiO_2 as a new ETL layer

Table. 3 comparisons between the performances simulated parameters of the device which using TiO_2

	J_{SC} (mA/cm^2)	V_{OC} (V)	FF (%)	PCE (%)
Blend with TiO_2	17.3542	1.16289	80.6211	16.2702
Blend with SnO_2	17.07	1.39	83.25	19.77

Conclusion

The SCAPS tool has been used to simulate and calibrate a dye-sensitized solar cell. The article makes a comparison between two theoretical configurations, blend and layer, to study the effect of changing the active layer structure on performance parameters. The influence of ETL and HTL thicknesses, working temperature, doping in ETL, electron mobility, and defect density at interface between active layer and HTM have been studied on the performance of the simulated cells. Simulated results show that the layer configuration is rather inconsistent in parameters behaviour with those for such cells experimentally recorded in earlier articles. While the blend structure has proved both, consistency and the attainment of the highest optimized performance values; J_{sc} of 17.3542 mA/cm^2, PCE of 16.2702 %, V_{oc} =1.16289 V, and FF =80.6211%. The authors have proposed a novel structure for the blend configuration to enhance its performance by replacing Tio_2 as the ETL layer with Sno_2. This is endorsed by its advantageous characteristic properties compared to other ETLs. Promising results from the new proposition are obtained with J_{sc} of 17.07 mA/cm^2, PCE of 19.77 %, FF of 83.25 % and V_{oc} of 1.39 V. These results can be used as a guide to producing higher performance DSSC structures.

Authors' Contributions

M. A. Abd El Ghany, M. D. Asham and Tarek M. Abdolkader wrote the main manuscript text. M. A. Abd El Ghany, M. D. Asham and W. Abdelaziz performed the simulation and prepared the figures. All authors shared in conceptualization, methodology and validation. All authors reviewed the manuscript.

References and Bibliography

[1] R. A. Afre and D. Pugliese, “Perovskite Solar Cells: A Review of the Latest Advances in Materials, Fabrication Techniques, and Stability Enhancement Strategies,” Micromachines, vol. 15, no. 2, 2024, doi: 10.3390/mi15020192.

[2] S. C. R. C. Christopher and C. X. Sahaya, “Modeling and Simulation of a Dye Sensitized Solar Cell with Porous Aerogel Photoanode,” J. Electr. Eng. Technol., vol. 16, no. 1, pp. 509–514, 2021, doi: 10.1007/s42835-020-00600-9.

[3] V. Rondan, G. F. Ayala, and M. D. Seuret, “New architecture in dye sensitized solar cells : a SCAPS - 1D simulation study,” Opt. Quantum Electron., vol. 52, no. 6, pp. 1–11, 2020, doi: 10.1007/s11082-020-02437-y.

[4] G. A. Nowsherwan et al., “Numerical optimization and performance evaluation of ZnPC : PC70BM based dye - sensitized solar cell,” Sci. Rep., pp. 1–16, 2023, doi: 10.1038/s41598-023-37486-2.

[5] P. Gnida, M. Libera, A. Paj, and E. Schab-balcerzak, “Examination of the E ff ect of Selected Factors on the Photovoltaic Response of Dye-Sensitized Solar Cells,” 2020, doi: 10.1021/acs.energyfuels.0c02188.

[6] A. Gunasekaran, H. Ying, V. K. Ponnusamy, and A. Sorrentino, “Synthesis of high polydispersity index polylactic acid and its application as gel electrolyte towards fabrication of dye - sensitized solar cells,” J. Polym. Res., 2021, doi: 10.1007/s10965-021-02615-w.

[7] T. Ouslimane, L. Et-taya, L. Elmaimouni, and A. Benami, “Heliyon Impact of absorber layer thickness , defect density , and operating temperature on the performance of MAPbI 3 solar cells based on ZnO electron transporting material,” Heliyon, vol. 7, no. November 2020, p. e06379, 2021, doi: 10.1016/j.heliyon.2021.e06379.

[8] W. Abdelaziz, A. Shaker, M. Abouelatta, and A. Zekry, “Possible efficiency boosting of non-fullerene acceptor solar cell using device simulation,” Opt. Mater. (Amst)., vol. 91, no. March, pp. 239–245, 2019, doi: 10.1016/j.optmat.2019.03.023.

[9] N. Chawki, “Numerical Study of BaZrS 3 Based Chalcogenide Perovskite Solar Cell Using SCAPS-1D Device Simulation,” pp. 1–18, 2022.

[10] W. Abdelaziz, A. Zekry, A. Shaker, and M. Abouelatta, “Numerical study of organic graded bulk heterojunction solar cell using SCAPS simulation,” Sol. Energy, vol. 211, no. October, pp. 375–382, 2020, doi: 10.1016/j.solener.2020.09.068.

[11] B. Rahman and H. Miah, “RSC Advances and hole transport layer for the mixed perovskite,” pp. 17130–17142, 2023, doi: 10.1039/d3ra02170j.

[12] L. Arumugam, P. L. L. B, M. E. Yeoh, and G. Thien, Simulation of Dye-Sensitised Solar Cell with Mesoporous Zinc Oxide Layer of Different Thicknesses and with Dye-Sensitisers. Atlantis Press International BV. doi: 10.2991/978-94-6463-082-4.

[13] N. Rai, S. Rai, P. Kumar, S. Pooja, and L. D. K. Dwivedi, “Analysis of various ETL materials for an efficient perovskite solar cell by numerical simulation,” J. Mater. Sci. Mater. Electron., vol. 1, no. 0123456789, 2020, doi: 10.1007/s10854-020-04175-z.

[14] R. García-Rodríguez, J. Villanueva-Cab, J. A. Anta, and G. Oskam, “A critical evaluation of the influence of the dark exchange current on the performance of dye-sensitized solar cells,” Materials (Basel)., vol. 9, no. 1, 2016, doi: 10.3390/ma9010033.

[15] L. Dissanayake and C. A. Thotawatthage, “The effect of TiO2 photo anode film thickness on photovoltaic properties of dye-sensitized solar cells The effect of TiO 2 photoanode film thickness on photovoltaic properties of dye-sensitized solar cells,” no. October, 2016, doi: 10.4038/cjs.v45i1.7362.

[16] F. Jahantigh and M. Javad, “The effect of HTM on the performance of solid - state dye - sanitized solar cells (SDSSCs): a SCAPS - 1D simulation study,” Appl. Phys. A, pp. 1–7, 2019, doi: 10.1007/s00339-019-2582-0.

[17] D. Lee, S. Thogiti, and J. H. Kim, “Effect of Temperature on the Photovoltaic Performance of Dye-Sensitized Solar Cells,” no. May, 2016, doi: 10.1166/sam.2016.2717.
[18] N. Sinha, P. Roy, D. S. Ghosh, and A. Khare, “Simulation and analysis of schottky junction perovskite solar cells (SJPSCs) Simulation and analysis of schottky junction perovskite solar cells (SJPSCs),” no. March, 2021, doi: 10.1088/1757-899X/1120/1/012017.
[19] S. G. El Gabaly et al., “Modeling the effect of functional groups on the electronic properties of benzene, pyridine and pyrimidine,” Egypt. J. Chem., vol. 62, pp. 15–17, 2019, doi: 10.21608/EJCHEM.2019.12903.1807.
[20] M. I. Attia, “Groundwater in Egypt,” Bull. Inst. Desert, Egypt, vol. 4, no. 1, pp. 198–213, 1954.
[21] Y. A. El-Shattory, A. M. G. El-Mawla, and H. A. A. El-Hamide, “Improved manual dishwashing liquid detergent compared to that produced by multinational companies in Egyptian market,” Egypt. J. Chem., vol. 61, no. 4, pp. 651–659, 2018, doi: 10.21608/EJCHEM.2018.2756.1222.